

How orbital angular momentum modes are boosting the performance of radio links

Timothy D. Drysdale¹ ✉, Ben Allen², Chris Stevens², Simon J. Berry³, Francis C. Smith³, Justin Coon²,

¹ School of Engineering and Innovation, The Open University, Walton Hall, Milton Keynes MK4 2BB, United Kingdom

² Department of Engineering Science, The University of Oxford, Parks Road, Oxford, OX1 3PJ, United Kingdom

³ Advanced Services and Products, QinetiQ, Cody Technology Park, Farnborough, GU14 0LX, United Kingdom

✉ E-mail: tim.drysdale@open.ac.uk

Abstract: This paper focuses on the application of orbital angular momentum (OAM) modes for enhancing radio communications. It is shown that OAM modes can enhance the spectral efficiency of line-of-sight links where there is limited or no diversity gain, and also increase physical layer security. Multiple-input multiple-output (MIMO) systems, in comparison, can struggle to give spectral efficiency improvements in line-of-sight links because they are not typically configured to exploit OAM modes. The concept of specifically using OAM modes shows great promise provided that several challenges are addressed. This paper aims to clarify OAM in the context of applications to which it is well suited, such as high capacity point-to-point links alongside transport infrastructure, within data centres, and between buildings.

1 Introduction

Wireless communications links are an attractive option for point-to-point backhaul applications where it is not practical or desirable to trench a physical cable. Backhaul links might involve (a) supporting transport infrastructure, where the number of connection points is too high to be implemented with fibre-optic cable, (b) live broadcast video links, where the link is only required temporarily, (c) data centres and complex sensor-actuator networks where the overall need for links is long-lived but they may need frequent reconfiguration to meet operational needs, (d) linking buildings such as on corporate or university campuses.

The limited availability of wireless spectrum constrains the bandwidth available to a wireless link, thus it becomes important to increase the spectral efficiency. For conventional mobile communications, spectral efficiency improvements are achieved by adding antennas and appropriate signal processing to exploit multiple propagation paths in the environment. Mobile phone and WiFi systems exploit this MIMO approach to good effect, because their users are concentrated in urban areas that contain a great deal of clutter. For point-to-point links, there is not always enough diversity in the propagation environment to allow a MIMO system to reach its full potential. Highly directional antennas have been used extensively in this context to good effect, but we show that this may be further improved upon through the exploitation of spatial modes. These are a subset of the modes available to a MIMO system. The difference between a spatial mode and a conventional radio mode is in the pattern of the phase as a function of space. To a first approximation, a conventional radio signal has a constant phase offset that is proportional to the distance between the transmitter and receiver. Using a scalar-wave analogy for simplicity, this results in a far field of the form:

$$A(r, t, \theta, \phi) \propto \frac{U(\theta, \phi)}{4\pi} \frac{e^{j(kr + \omega t)}}{r} \quad (1)$$

where A is the complex magnitude of the far field, U is the magnitude of the transmitter's radiation pattern as a function of azimuth ϕ and elevation θ , r is distance between the transmitter and the receiver, t is the time dependence, ω is the instantaneous frequency and k is the propagation constant.

On the other hand, a spatial mode has a non-uniform phase pattern, ψ , imposed upon it that varies as a function of the azimuth (ϕ) and elevation (θ) relative to the transmitter:

$$A(r, t, \theta, \phi) \propto \frac{U(\theta, \phi)}{4\pi} \frac{e^{j(kr + \omega t + \psi(\theta, \phi))}}{r} \quad (2)$$

For enhancing the spectral efficiency of a communications link, a set of mutually independent spatial modes is required. The maximum potential increase in spectral efficiency relates to the number of independent spatial modes that can be transmitted and received simultaneously, for a given spectral band. As an alternative, spatial modes can be used directly as symbols, so to enhance security by increasing the cost to the adversary of eavesdropping. This paper concentrates on a set of independent modes, the so-called OAM modes, which is theoretically infinite. Despite their promise, there are a number of practical considerations that must be understood and addressed in order to exploit their potential.

2 What are OAM modes?

Orbital angular momentum modes are characterised as having a helical phase structure with the axis of rotation along the boresight. The amplitude pattern typically has a null along the boresight of the antenna due to the screw dislocation caused by the phase pattern. The helical phase structure is characterised according to the amount of phase accumulated in one rotation around the plane perpendicular to the boresight direction. While the phase offset is fixed as per Eq. 2, when viewed as a sequence of snapshots in time, the modes appear to rotate at the angular frequency of the supporting wave ω .

This is restricted to being an integer multiple of 2π , so the total phase change in one revolution around the boresight is given as $\oint \psi = 2\pi l$ where l is the mode number, which can be positive, negative, or zero. Thus the phase modification from Eq. 2 is given for an ideal OAM mode by

$$\psi(\theta, \phi) = l\phi, \quad (3)$$

although in practice the OAM modes produced by antennas also have a slight dependence on θ . While fractional OAM modes exist [1], they have an additional dislocation in the pattern and fall outside the scope of the present discussion.

Figure 1(a,b) shows an example of the magnitude and phase of an OAM mode produced by a uniform circular array antenna. In Fig. 1(a), the magnitude plot shows an annular ring, where there is little or no signal transmitted along the boresight. The phase plot

in Fig. 1(b) shows a distinctive spiral pattern. Conceptual illustrations of the degree of helicity associated with some example mode numbers as shown in Fig. 1(c).

2.1 Relationship to polarisation

In general, the angular momentum of a wave comprises independent components of spin angular momentum (SAM) and OAM, one or both of which may be zero or non-zero depending on the transmitting antenna properties. Circularly polarised waves have SAM, while a linear polarised wave does not. Either can have an OAM component. In other words, OAM is independent to polarisation, so OAM modes can be imposed onto waves of any arbitrary polarisation whether linear, elliptical, or circular. This allows polarisation to be fully exploited [2]. Note that a conventional MIMO system would have spatial modes, but the linear or planar arrays typical of current implementations for mobile phones and wifi are not well suited to producing OAM modes as a consequence of the non-circular array geometry.

Figure 2 shows the electric field vector at snapshots in time (at intervals equivalent to the time taken to travel an eighth of a wavelength) as a plane wave propagates along a direction z . In Fig. 2(a) the wave is circularly polarised only, and has no OAM. The electric field vectors in each snapshot are oriented in the same direction. In Fig. 2(b), the wave now has OAM of mode 1 superimposed upon it. The electric field vectors are now no longer all oriented uniformly, although they all continue to rotate at the same rate. The difference is that the rotational position of each vector is offset by an amount equal to the phase of the helical phase pattern that comprises the OAM mode.

3 Evolution of research in the field

OAM modes first came to the attention of optical physicists studying the properties of Laguerre-Gaussian laser beams in 1992 [3]. The mechanical equivalence of the angular momentum of light was soon demonstrated in experiments with particles trapped in so-called optical tweezers [4, 5], which highlighted that light with OAM had distinct properties not available purely from circular polarisation (SAM). In these experiments, the OAM mode was produced by reflecting the laser beam off of a spatial light modulators that had been programmed with an appropriate hologram. The tunability of the hologram then led to the demonstration of secure information transmission using data encoded in OAM modes, over optical free-space links of 15m length in 2004 [6].

The concept was explored for use at radio frequencies shortly afterwards in 2007 [7], provoking discussion in the radio communications community over the relationship between OAM modes and the modes available to MIMO systems [8, 9]. Since OAM modes can be generated and detected with multiple antennas, then it is possible to apply to them the same channel capacity calculations that are used for MIMO systems. When this is done, it becomes clear that OAM-based communications links are subject to the same fundamental channel capacity limits, but have the potential to deliver high performance at short distance with low computational complexity [8]. One can view OAM modes as being a subset of the modes available to MIMO systems. However, not all MIMO modes are available to all MIMO systems. For example, 4×4 MIMO systems have modes that are not available to a 2×2 MIMO system. In the same way, conventional MIMO implementations that have been designed for use in mobile and wifi applications are not well suited for accessing OAM modes in their operation. For example, two-antenna systems cannot generate OAM modes at all, while four-antenna systems could potentially generate OAM modes of the first order ($|l| = 1$) but no higher, and even then only if suitable signal processing facilities are available for beamforming. MIMO implementations are typically optimised for mobile and WiFi applications, so it is unreasonable to expect them to perform as well in line-of-sight point-to-point links, because they will not be able to exploit enough OAM modes to make up for the lack of diversity gain. This motivates the study of systems that are optimised to utilise OAM

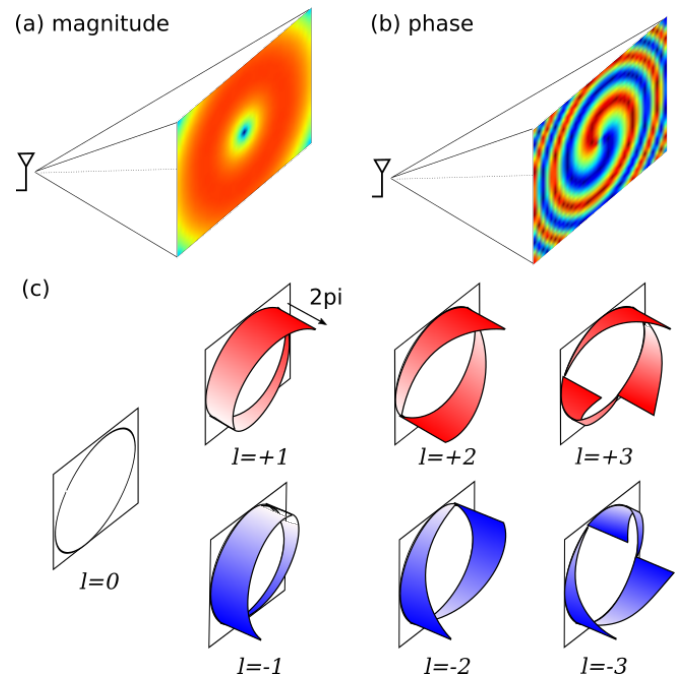


Fig. 1: Illustrations of OAM modes, with a plot of the farfield (a) magnitude and (b) phase for mode $l=+1$, and (c) conceptual illustrations of the phase at peak gain for a number of modes.

modes. In other work, it was reported that the mode density of OAM was insufficient for significant capacity gain [10] but this is countered by work in optics where more than 50 OAM modes have been simultaneously transmitted [11].

Using OAM modes in radio links relies on being able to encode data [12, 13]. The benefit of using OAM in line-of-sight links was demonstrated in 2014 with a 32 Gbit s^{-1} link operating in the 28 GHz band, achieving a spectral efficiency of $\sim 16 \text{ bit } s^{-1} \text{ Hz}^{-1}$ through multiplexing data onto four independent OAM modes on each of two orthogonal linear polarisations. The link was only 2-3 m, and the overall structure was large, because there were separate horn antenna for each mode.

Subsequently, interest in the field has blossomed. For example, demonstrations have shown that multiplexed OAM modes can be steered analogously to regular beams [14]. While the presence of a reflector can degrade the mode pattern in some circumstances [15], in other cases it may be that obstructions can be handled by placing them in the null [16]. Now the goal is finding alternative transmit and receive approaches that are smaller in size, and that can support longer link distances.

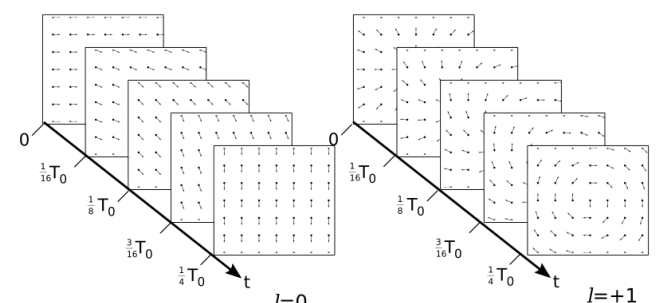


Fig. 2: Plot of the electric field vector at snapshots in time as a plane wave propagates (a) circular polarisation alone, (b) circular polarisation with OAM mode 1.

4 Generation of OAM modes

OAM modes can be generated using a number of approaches, as shown in Fig. 3.

4.1 Spiral phase plates

Figure 3(a) shows a dielectric holographic element, a spiral phase plate (SPP). SPPs usually operate in transmission mode, and directly imposes the required helical phase pattern onto the transmitted wavefront. SPPs can be machined from an appropriate low-loss polymer or additively manufactured with 3D printing techniques, either in one piece or several [17]. The surface relief depth, d , of a SPP made of a dielectric with refractive index n can be calculated as a function of position (x, y) and mode number l as follows:

$$d(x, y) = \frac{\text{mod}(l \cdot \arctan2(y, x) + \pi, 2\pi)}{k_0(n - 1)}, \quad (4)$$

where $k_0 = 2\pi/\lambda_0$ is the wavenumber of the carrier wavelength λ_0 . The design equation is only strictly valid at one frequency, but in practice SPPs have sufficient bandwidth for use in communications channels. For example, a SPP designed for operation 60 GHz would produce an error of 1% in the mode, at the edges of a 1.2 GHz bandwidth channel.

SPPs can also be used in reflection mode. For example, a parabolic dish can be cut and bent to produce a reflection-mode SPPs [18]. With appropriate compensation in the phase profile, planar reflection-mode SPP can also be used with off-set feeds, as demonstrated at 94 GHz [19]. A recent report suggested that an additional degree of freedom could be obtained from rotating the SPP although the available incremental data capacity is limited by practical considerations relating to the maximum speed of rotation [20].

4.2 Uniform circular array

Uniform circular arrays (UCAs) are a natural starting point for the study of antennas that transmit and receive OAM modes, because they share the same rotational symmetry. In a UCA, the elements are spaced around the circumference of a circle of radius R [8], as shown in Fig. 3(b). The signal to the n^{th} element is phase shifted by $\psi(n)$, given by

$$\psi(n) = l \cdot \theta_n \quad (5)$$

where l is the mode number and θ_n is the azimuthal position of the n^{th} element relative to the centre of the array. One or more rings of elements can be used, and the maximum resolvable mode number is $|l| < N/2$ where N is the total number of antenna elements in a single ring array [7].

Aside from phase shifters, the required phase shifts can also be achieved using delay lines [21], or switches [22]. When switches are used, the mode number increases with the harmonic of the switching frequency. In an analogous manner, the mode number can be tuned as a function of frequency if the position of the antenna elements is laid out on a helical path [23]. Such an approach has relevance in adding elevation discrimination to radar, but may need additional development to support efficient multiplexing. A Rotman lens was used to simultaneously produce five OAM modes in a nine-element array UCA where $l \in \{0, \pm 1, \pm 2\}$ at 7.9 GHz [24]. The prototype was reported to have measured return loss better than -10 dB over a bandwidth of 0.6 GHz but the mode purity was only shown for the central frequency.

4.3 Resonator-based feed systems

A ring resonator was used to generate two OAM modes simultaneously, which were then focused by a parabolic reflector in [25]. An alternative was proposed in [26], which can produce four modes simultaneously ($l \in \{\pm 3, \pm 13\}$), and is made more compact through the use of a Bull's eye structure, as shown in Fig. 3(c),

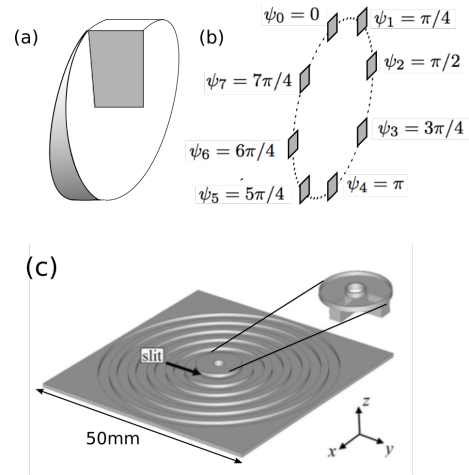


Fig. 3: Illustrations of methods for generating OAM modes (a) spiral phase plate, (b) uniform circular array, and (c) ring resonator feed and bull's eye surface

instead of the parabolic reflector. A related approach involves using a dielectric resonator element instead of a metallic ring resonator [27], while omni-directional patterns can be produced by using a parallel-plate feed [28]. These resonator-based antennas support two opposite handed modes of the same mode number in each resonator, whereas a SPP can only generate one mode. This makes resonator based systems potentially more attractive for communications applications where multiple modes are required. Developments are required to further enhance the multiplexing capabilities of OAM antennas.

5 OAM properties

OAM modes exhibit some characteristic properties, such as a null along the boresight that diverges with distance. The angle of divergence also increases with the absolute value of the mode number. The null size, or divergence angle, limits the practical link distance, and hence is an important figure of merit.

5.1 Null size

The null size can be described in terms of a divergence angle α , that represents the angle from the boresight to the maximum gain of the mode. The ratio of the divergence angle for two different mode numbers l_2 and l_1 , where $|l_2| > |l_1|$ is related to the absolute values of the mode numbers and the standard deviation of the spatial distribution of the beams, which is given by the square root of the radial variance of the intensity distribution [29]:

$$\frac{\alpha_{l_2}}{\alpha_{l_1}} = \frac{(|l_2| + 1)r_{\text{rms}}^{l_2}(z)}{(|l_1| + 1)r_{\text{rms}}^{l_1}(z)}, \quad (6a)$$

$$r_{\text{rms}}^{l_n} = \sqrt{2\pi \int_0^\infty r^2 I_{l_n}(r, z) r dr}. \quad (6b)$$

According to Eq. 6, the divergence angle scales as

$$\frac{\alpha_{l_2}}{\alpha_{l_1}} = \left(\frac{|l_2|}{|l_1|} \right)^p \quad (7)$$

where the limiting values of the exponent are $0.5 \leq p \leq 1.0$, with $p = 0.5$ equating to the modes both having a constant beam waist (from the perspective of being a Laguerre-Gaussian mode). The other limiting value of $p = 1.0$ equates to the modes having the same standard deviation of the spatial distribution. If different size apertures are used to generate each mode, the value falls between

the limiting values [26]. The value of p cannot be computed without measuring or calculating the far-field mode patterns. Along with divergence angle, another useful figure of merit quantifies the quality of the phase profile.

5.2 Mode purity

The quality of an OAM mode can be assessed by comparing the actual phase difference between two receive points, to the expected phase difference. It is important for a mode to have good quality, so that it can be received efficiently, and without leaking energy into the other modes. To evaluate the mode purity, the so-called phase gradient method uses two antennas located on a circle of fixed radius and gives an estimate of the received mode as

$$l_R = \frac{\phi_1 - \phi_2}{\beta_{1,2}} \quad (8)$$

where ϕ_1 and ϕ_2 are the phases of the signals from the two receivers and $\beta_{1,2}$ is the angle formed by the two receivers with respect to the centre of the circle [30]. For discrimination between modes to be possible, the received mode should fall within a range of ± 0.5 mode numbers.

5.3 Independence

For communications applications, data capacity can be enhanced if independent modes are available. If the modes are not fully independent, then the signal-to-interference ratio increases, reducing the system capacity. In principle, all OAM modes are mutually independent, so long as the whole mode is received. On the other hand, if the receiver's aperture only overlaps with a part of the mode, then modes can be aliased and the signal-to-interference ratio can rise to unacceptable levels. For a receiver with a continuously-sampled partial aperture of angle $2\pi/b$ where b is a free parameter, the independence of two modes can be evaluated as follows [31]:

$$V = \frac{b}{2\pi} \int_0^{2\pi/b} e^{j(l_1 - l_2)\phi} d\phi = \begin{cases} 1 & l_1 = l_2 \\ 0 & l_1 - l_2 = b \cdot m \\ > 0 & \text{otherwise} \end{cases} \quad (9)$$

where m is a free parameter that must be an integer. When Eq. 9 gives $V = 0$, it indicates that the two modes are independent. For radio applications, it is more likely that the receiver aperture is discretely sampled using antenna elements, in which case the independence criteria can relax, so long as the partial aperture is sampled appropriately, with an uneven spacing [26] or two pairs of receivers [32].

6 Modelling and measuring mode patterns

The mode patterns are straightforward to calculate and require no special analysis methods, so long as the phase of any signals fed to the antenna is preserved. Thus conventional modelling techniques such as the finite element method and the finite difference time domain technique can be used. For antenna arrays, the mode patterns can be calculated using a quasi-analytical approach. Assuming isotropic elements with uniform magnitude U_0 , and suppressing the time dependence, the far field is:

$$A(r, \theta, \phi) = \sum_{n=0}^{N-1} 4U_0 \pi \frac{e^{j(kr + \psi_n)}}{r} \quad (10)$$

where r is the distance from the transmitter to the receiver, ψ_n is the phase offset applied to the signal fed to the n^{th} transmit antenna, and k is the wavevector. Example far-field mode patterns resulting from Eq. 10 for an eight element UCA at 5 GHz with diameter of $3\lambda=18$ cm are plotted in a 1.4×1.1 m plane at the nearest extent of

the far-field ($z = 2.16$ m), with the magnitude in Fig. 4(a) and the phase in Fig. 4(b). A noise floor has been applied to the simulated magnitude results, at -32 dB from the peak value, so as to make clear how the null size grows with mode number.

Mode patterns can be measured using 2D or 3D field scanning methods. To demonstrate this, we have used a field scanning system with a coaxial probe to record the field in steps of 44 mm by 39 mm across a 1.4×1.1 m plane at 5 GHz for the same UCA. The measured magnitude is shown in Fig. 4(c), and the phase in Fig 4(d). The measured mode patterns show good agreement to the simulated results for mode numbers $l \in \{0, \pm 1, \pm 2\}$. For $l = \pm 3$, the null is large and there is little signal available within our scanning plane, reducing the quality of the phase pattern significantly. This result highlights the practical constraints on the receive antenna size that are imposed by the boresight null that is characteristic of OAM modes.

7 Partial aperture detection

The size of OAM mode patterns grows with link distance, due to the non-zero divergence angle. Practical implementations of OAM links will require effort toward smaller receive antenna array sizes, whilst maintaining the information capacity of the link. Partial aperture receivers are such an example. A partial aperture receiver has a smaller size but can cause modes to alias onto one another as indicated in Section 5.3. A discretely sampled partial aperture requires carefully chosen positioning of the receive elements so as to retain the independence of the modes for detection.

We can demonstrate this experimentally by comparing the performance of two different four element receive arrays, together with the transmitter that produced the modes in Fig. 4(c,d). The measured results in this section were obtained in a $2.5 \times 2.5 \times 4.0$ m radio frequency anechoic chamber. In each case, the transmitter and receiver were 2.37 m apart (the boundary with the near field is 2.16 m). A photograph of the experimental setup is shown in Fig. 5.

Two different receiver designs were tested; one with uneven spacing, discretely-sampled partial-aperture receiver (DSPAR), that was optimised according to [26], and one with uniform spacing for comparison, uniformly-sampled partial-aperture receiver (USPAR), as shown in Table 1. In each case, the four receive antennas were positioned on an arc of radius 0.5 m for all four designs. The antenna positions can be interpreted with the aid of the diagram in Fig. 6. Note that the bypass antenna is on the boresight, and is in the same place for all experiments. It is not part of the receiver, but simply used for alignment of the transmitter.

Table 1 Channel sounding test parameters.

Test No.	Modes	Receiver type	Antenna positions
1	$(\pm 1, \pm 2)$	DSPAR	$0^\circ, 56^\circ, 129^\circ, 187^\circ$
2	$(\pm 1, \pm 2)$	USPAR	$0^\circ, 60^\circ, 120^\circ, 180^\circ$

The results of the experiment are shown in Fig. 7. The measurements are intended to replicate the performance of a system that is transmitting on four OAM modes at once. Therefore there are four receivers, one for each OAM mode. Each receiver also receives all four signals at the same time, but only wants one of them. When the transmitter mode number matches the receiver mode number, the amount of signal received should reach a maximum compared to the three other modes. The process is repeated with the receiver set to each of the other modes. There are sixteen results in all, per receiver design. These are plotted as a 3-D bar chart, with one axis representing the transmit mode and the other representing the receive mode. The results for each receiver are normalised to the largest signal received, whether it is the desired mode or not. The large green

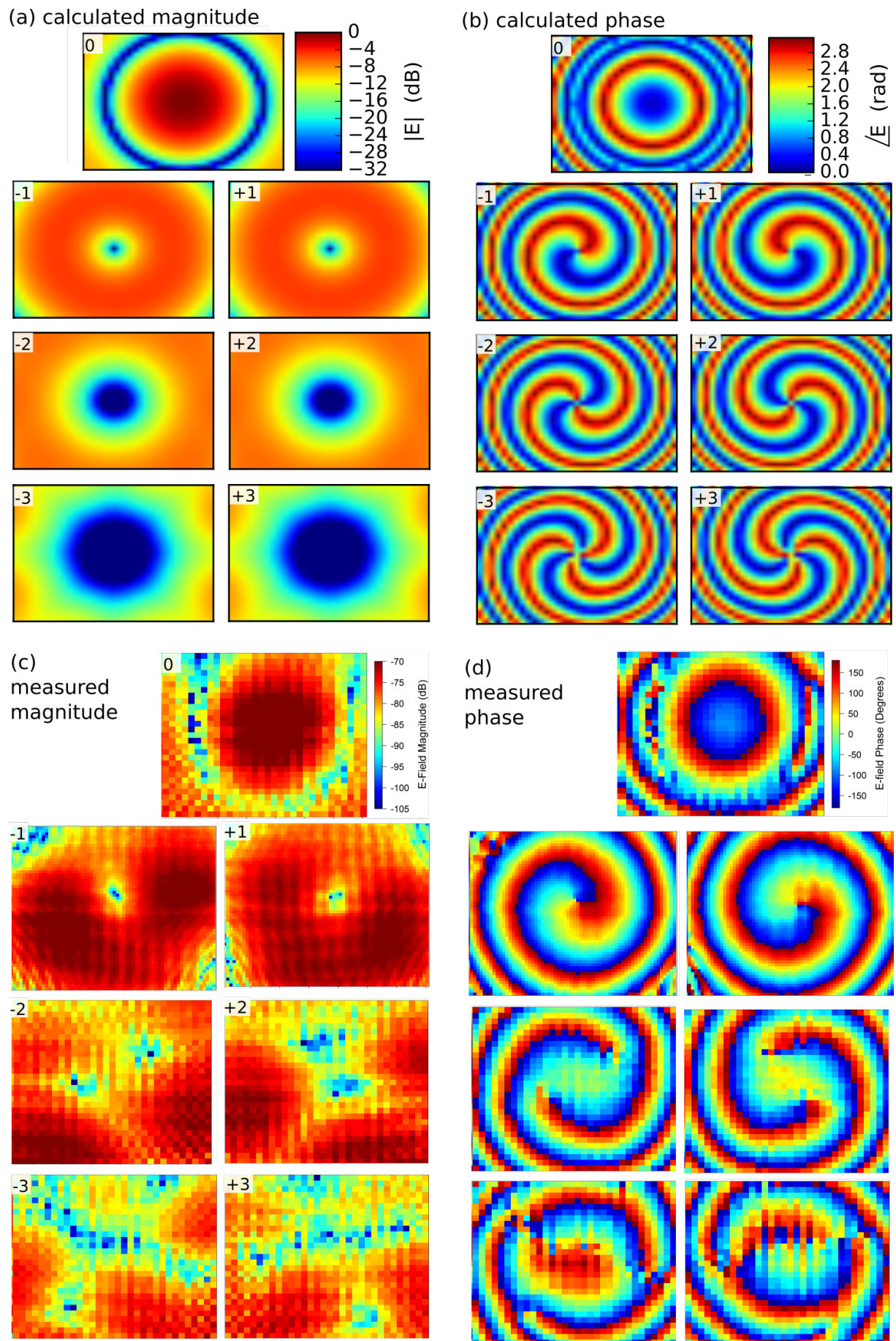


Fig. 4: Far field mode patterns for an eight element uniform circular array of diameter $3\lambda = 18$ cm at 5 GHz

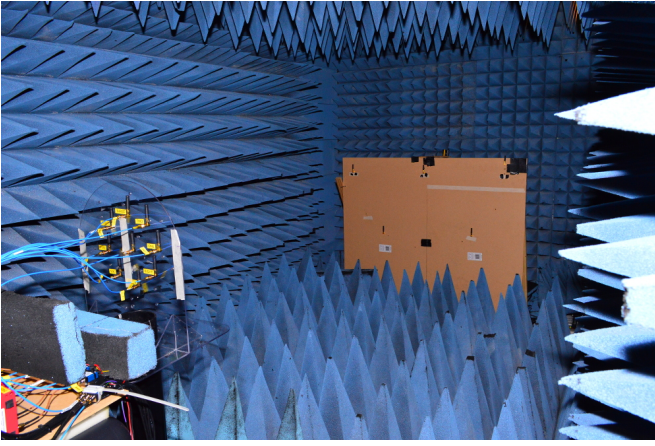


Fig. 5: Photograph of the transmitter and receiver during the channel sounding experiments. The receiver is in the far field, at a distance of 2.37 m

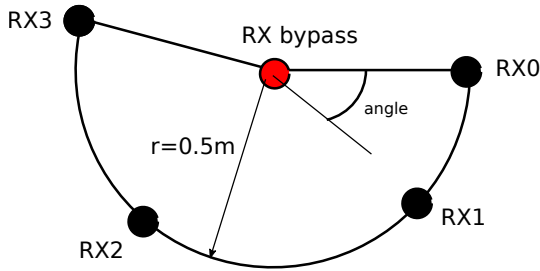


Fig. 6: Schematic illustration of the antenna positions

bars represent the desired mode being received as the strongest signal - ideally there should be four green bars per chart, that appear along the diagonal. This is the case for the DSPAR designs.

The uniformly spaced receiver USPAR does not exhibit this behaviour - at least two channels in each case show magenta bars representing a desired mode that is smaller than at least one of the crosstalking modes. In other words, the USPAR design is not adequate for the task of receiving multiple modes, and optimised designs must be used.

We can analyse the results from the experiment in some more detail to establish the bandwidth of the modes, and then infer the channel capacity for a full four-channel system using Shannon-Hartley theorem, which is:

$$C = B \log_2 \left(1 + \frac{S}{N} \right) \quad [\text{bit/s/Hz}] \quad (11)$$

where C is the channel capacity in bits per second per hertz, B is the bandwidth of the channel in hertz, and $\frac{S}{N}$ is the average linear signal-to-noise ratio (SNR). Eq. 11 holds for band-limited channels with average white Gaussian noise under a mean power constraint. It is a topic of future investigation to determine the cross-talk statistics and refine resulting capacity estimate.

The measured signal to noise ratio* can be evaluated at each frequency point for which data was captured. This can be done by dividing the power received in the desired OAM mode, $P_{u,u}$, by the sum of the power received in the three undesired modes ($P_{-u,u}$, $P_{v,u}$, and $P_{-v,u}$) where $l \in \{u, -u, v, -v\}$ are the four OAM mode numbers chosen for the link. The first subscript is the mode number at the transmitter, while the second subscript is the mode

*which could also be thought of as a signal to interference ratio in this case

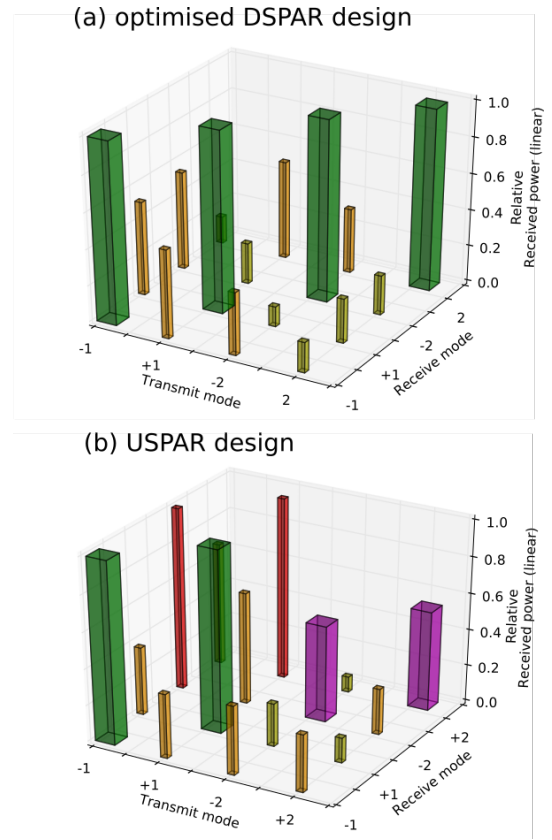


Fig. 7: Crosstalk results from the channel sounding measurements

number at the receiver, thus:

$$\text{SNR} = \frac{P_{u,u}}{P_{-u,u} + P_{v,u} + P_{-v,u}}. \quad (12)$$

The measured SNR for each of the four received OAM modes is plotted as a function of frequency in Fig. 8. The total capacity is estimated by substituting the values for SNR into Eq. 11 to obtain the individual capacity of each of the four channels, and then summing the four individual channel capacities to give a total link capacity. The measured results indicate a total link capacity of 16.0 Gbps across the 2 GHz bandwidth of the experiment. The bandwidth was limited by the programmable phase shifters. Such a wide bandwidth could not be readily obtained outdoors because of existing wireless spectrum allocations, but it validates the use of OAM modes across wide bandwidths. This is relevant because wider bandwidths are available in other bands, such as millimetre-wave bands. The designed receiver's theoretical capacity was calculated to be higher, at 29.5 Gbps, because it was assumed to be operating under ideal conditions (and thus excluded effects such as the non-isotropic frequency-dependent radiation pattern of the individual antenna elements, mutual coupling between the elements, and slight imbalances in the magnitude and phase of the signal applied to each element).

Table 2 Measured and designed linear SNR and link capacity

Received mode:	-1	+1	-2	+2	Total capacity
Measured SNR	3.1	3.9	1.9	3.4	16.0 Gbps
Designed SNR	19.8	19.8	7.1	7.1	29.5 Gbps

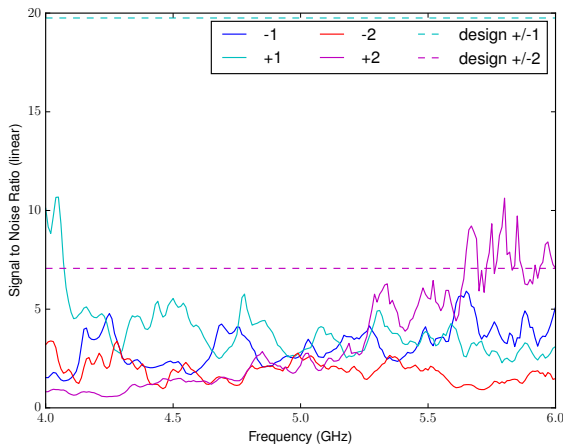


Fig. 8: Measured linear signal-to-noise ratio as a function of frequency, for each received mode, for the best performing receiver we tested.

8 Application

The additional degree of freedom provided by OAM modes can be used either to enhance the security of the channel, or enhance the spectral efficiency, or a combination of both.

8.1 Security

The security of a wireless link can be enhanced by making it more challenging for eavesdroppers to obtain a useful signal. An eavesdropper is likely to be restricted to locations that lie off of the axis of the link, because they will not have access to the full mode pattern and are more likely to suffer aliasing because of the partial aperture effect described in Eq. 9. They will be unable to adequately sample the transmitted mode and will not be able to distinguish between different OAM modes. Thus a signal that is comprised of symbols derived from OAM modes, and their combinations, will be unreadable. An alternative method is to transmit an encrypted data stream using a conventional radio mode (or an OAM mode), but transmit (for example) the key on an additional OAM channel. As before, an eavesdropper would be disadvantaged by being unable to read the data that is carried on the OAM channel. A quantitative analysis of the security applications of OAM is outside the scope of this paper.

8.2 Spectral efficiency

When multiple OAM modes are used simultaneously, the spectral efficiency of a transmission can be enhanced compared to a single-input single-output (SISO) link. Compared to a conventional MIMO system, the benefit in explicitly targeting OAM modes comes when the propagation environment has little diversity gain, such as in a static line-of-sight link. A further benefit of OAM links appears to be the reduction in the overall size of the antenna arrays that is required to achieve a given data capacity [33], compared to conventional MIMO systems.

8.3 High-data rate relays

The spectrally efficient characteristics of a single OAM link over short-to-medium distances can be exploited in a relay network to create a high-capacity long-range backhaul network. The relay topology in this example would be linear, i.e., point-to-point OAM links would be concatenated to form one long multihop channel that connects the source to the destination. At each node (relay) in the system, the message could be demodulated and decoded before being re-encoded and transmitted along the next hop. This is the standard

decode-and-forward methodology that has been proposed for coverage extension in LTE networks. Other forwarding protocols exist (e.g., amplify-and-forward); how to appropriately choose the forwarding mechanism for a given OAM application is an open research problem.

In addition to unidirectional source-to-destination relaying, the inherent separability of OAM modes suggests that it would be suitable for full duplex, bidirectional relaying. In a backhaul setting, this would enable high-capacity uplink and downlink transmissions to take place simultaneously.

9 Conclusion

OAM modes are a type of spatial mode that can be used to enhance the spectral efficiency, or security, of a static line-of-sight wireless radio link. The main benefit of using OAM modes is that they do not require diversity gain. Demonstrations to date have shown link capacities of up to 32 Gbps, but only over a 2 m distance, and with bulky transmitters and receivers.

A spatial mode has some variation in the phase of the signal that varies as a function of position. An OAM mode's phase varies in helical manner. The appearance of a twisting action only arises from the combination of the phase offset from the radiation pattern, and the time dependence of the instantaneous phase. The mode number describes the number of branches in the phase pattern, which is the same as the total phase integrated around the circumference of the mode and divided by 2π . Modes can be left- or right-handed, depending on which direction the phase increments.

At present the link distance is limited because OAM modes diverge, requiring the receive aperture to increase with link distance. The divergence results in a null on the boresight. The divergence angle also increases with mode number, causing a larger null. This can be partly ameliorated by using partial aperture receivers, although this can impact on the choice of modes that can be used simultaneously.

In principle, all OAM modes are independent to each other. If the receive antenna is limited to a partial aperture, then some modes can alias onto others, creating crosstalk. With the use of appropriately located receive elements, independence can be restored. Mode patterns were measured for an eight element uniform circular array in the 4 - 6 GHz band, giving magnitude and phase patterns that agreed well with the calculated patterns. Then, four-element receive antennas were compared for cases with optimised, and unoptimised element positions. The optimised element positions reduced crosstalk. The modes exhibited wide bandwidth, and total channel capacity was estimated at 16 Gbps for the measured system over its 2 GHz bandwidth.

Future work in the field is expected to focus on methods for increasing the maximum link distance. Potential applications include wireless backhaul alongside transport infrastructure, links between racks in data centres, and between buildings on corporate or university campuses.

10 Acknowledgments

Tim Drysdale acknowledges funding from HM Govt and the Department for Transport's T T-TRIG fund, and thanks Sajad Haq and Chris Lawrence at QinetiQ for arranging access to their experimental facilities for mode scanning, and The Open University's acoustic anechoic chamber for access for test preparation. Ben Allen acknowledges the support of a Royal Society Industrial Fellowship under award number IF160001.

11 References

- Götte, J.B., O'Holleran, K., Preece, D., Flossmann, F., Franke, Arnold, S., Barnett, S.M., et al.: 'Light beams with fractional orbital angular momentum and their vortex structure', *Opt Express*, 2008, **16**, (2), pp. 993–1006
- Yan, Y., Xie, G., Lavery, M.P.J., Huang, H., Ahmed, N., Bao, C., et al.: 'High-capacity mm-wave communications with orbital angular momentum multiplexing', *Nat Commun*, 2014, **5**

- 3 Allen, L., Beijersbergen, M.W., Spreeuw, R.J.C., Woerdman, J.P.: 'Orbital angular momentum of light and the transformation of Laguerre-Gaussian laser modes', *Phys Rev A*, 1992, **45**, (11)
- 4 Simpson, N.B., Dholakia, K., Allen, L., Padgett, M.J.: 'Mechanical equivalence of spin and orbital angular momentum of light: an optical spanner', *Opt Lett*, 1997, **22**, (1), pp. 52–54
- 5 Padgett, M.J.: 'Light's twist', *Proc R Soc A*, 2014, **470**, (20140633)
- 6 Gibson, G., Courtial, J., Padgett, M.J., Vasnetsov, M., Pas'ko, V., Barnett, S.M., et al.: 'Free-space information transfer using light beams carrying orbital angular momentum', *Opt Express*, 2004, **12**, (22), pp. 5448–5456
- 7 Thidé, B., Then, H., Sjöholm, J., Palmer, K., Bergman, J., Carozzi, T.D., et al.: 'Utilization of photon orbital angular momentum in the low-frequency radio domain', *Phys Rev Lett*, 2007, **99**, pp. 087701
- 8 Edfors, O., Johansson, A.J.: 'Is OAM-based radio communication an unexploited area?', *IEEE Trans Ant & Propag*, 2012, **60**, (2), pp. 1126–1131
- 9 Willner, A.E., Ren, Y., Xie, G., Yan, Y., Li, L., Zhao, Z., et al.: 'Recent advances in high-capacity free-space optical and radio-frequency communications using orbital angular momentum multiplexing', *Phil Trans R Soc A*, 2017,
- 10 Andersson, M., Berglind, E., Björk, G.: 'Orbital angular momentum modes do not increase the channel capacity in communication links', *New Journal of Physics*, 2015, **17**, (4), pp. 043040
- 11 Lavery, M.P.J., Robertson, D.J., Sponselli, A., Courtial, J., Steinhoff, N.K., Tyler, G.A., et al.: 'Efficient measurement of an optical orbital-angular-momentum spectrum comprising more than 50 states', *New Journal of Physics*, 2013, **15**, (1), pp. 013024
- 12 Mahmouli, F.E., Walker, S.D.: '4-gbps uncompressed video transmission over a 60-ghz orbital angular momentum wireless channel', *IEEE Wireless Communications Letters*, 2013, **2**, (2), pp. 223–226
- 13 Allen, B., Tennant, A., Bai, Q., Chatziantoniou, E.: 'Wireless data encoding and decoding using oam modes', *Electronics Letters*, 2014, **50**, (3), pp. 232–233
- 14 Xie, G., Zhao, Z., Yan, Y., Li, L., Ren, Y., Ahmed, N., et al.: 'Demonstration of tunable steering and multiplexing of two 28 ghz data carrying orbital angular momentum beams using antenna array', *Scientific Reports*, 2016, **6**, pp. 37078 EP –
- 15 Yan, Y., Li, L., Xie, G., Bao, C., Liao, P., Huang, H., et al.: 'Multipath effects in millimetre-wave wireless communication using orbital angular momentum multiplexing', *Scientific Reports*, 2016, **6**, pp. 33482 EP –
- 16 Ahmed, N., Zhao, Z., Li, L., Huang, H., Lavery, M.P.J., Liao, P., et al.: 'Mode-division-multiplexing of multiple besel-gaussian beams carrying orbital-angular-momentum for obstruction-tolerant free-space optical and millimetre-wave communication links', *Scientific Reports*, 2016, **6**, pp. 22082 EP –
- 17 Schemmel, P., Pisano, G., Maffei, B.: 'Modular spiral phase plate design for orbital angular momentum generation at millimetre wavelengths', *Opt Express*, 2014, **22**, (12), pp. 14712–14726
- 18 Tamburini, F., Mari, E., Sponselli, A., Thidé, B., Bianchini, A., Romanato, F.: 'Encoding many channels on the same frequency through radio vorticity: first experimental test', *New Journal of Physics*, 2012, **14**, (3), pp. 033001
- 19 Cheng, L., Hong, W., Hao, Z.C.: 'Design and implementation of planar reflection spiral phase plate for beams with orbital angular momentum', *IET Microwaves, Antennas Propagation*, 2017, **11**, (2), pp. 260–264
- 20 Zhang, C., Ma, L.: 'Millimetre wave with rotational orbital angular momentum', *Scientific Reports*, 2016, **6**, pp. 31921 EP –
- 21 Bai, Q., Tennant, A., Allen, B.: 'Experimental circular phased array for generating OAM radio beams', *Electron Lett*, 2014, **50**, (20), pp. 1414–1415
- 22 Tennant, A., Allen, B.: 'Generation of OAM radio waves using circular time-switched array antenna', *Electron Lett*, 2012, **48**, pp. 1365–1366(1)
- 23 Yuan, T., Cheng, Y., Wang, H.Q., Qin, Y.: 'Generation of oam radio beams with modified uniform circular array antenna', *Electronics Letters*, 2016, **52**, (11), pp. 896–898
- 24 Bai, X.D., Liang, X.L., Li, J.P., Wang, K., Geng, J.P., Jin, R.H.: 'Rotman lens-based circular array for generating five-mode oam radio beams', *Scientific Reports*, 2016, **6**, pp. 27815 EP –
- 25 Hui, X., Zheng, S., Chen, Y., Hu, Y., Jin, X., Chi, H., et al.: 'Multiplexed millimeter wave communication with dual orbital angular momentum (oam) mode antennas', *Scientific Reports*, 2015, **5**, pp. 10148 EP –
- 26 Vourch, C.J., Drysdale, T.D.: 'V-band Bull's eye antenna for multiple discretely steerable beams', *IET Microw, Ant & Propag*, 2016, **10**, pp. 318–325(7)
- 27 Pan, Y., Zheng, S., Zheng, J., Li, Y., Jin, X., Chi, H., et al.: 'Generation of orbital angular momentum radio waves based on dielectric resonator antenna', *IEEE Antennas and Wireless Propagation Letters*, 2017, **16**, pp. 385–388
- 28 Quinlan, T., Walker, S.: 'A monopole fed omnidirectional 13dbi gain bi-conical horn antenna for ieee802.11ad applications'. In: 2016 Loughborough Antennas Propagation Conference (LAPC). (, 2016, pp. 1–4
- 29 Padgett, M.J., Miatto, F.M., Lavery, M.P.J., Zeilinger, A., Boyd, R.W.: 'Divergence of an orbital-angular-momentum-carrying beam upon propagation', *New Journal of Physics*, 2015, **17**, (2), pp. 023011
- 30 Mohammadi, S.M., Daldorff, L.K.S., Forozesh, K., Thidé, B., Bergman, J.E.S., Isham, B., et al.: 'Orbital angular momentum in radio: Measurement methods', *Radio Science*, 2010, **45**, (4), pp. n/a–n/a. rS4007
- 31 Zheng, S., Hui, X., Zhu, J., et al.: 'Orbital angular momentum mode-demultiplexing scheme with partial angular receiving aperture', *Opt Express*, 2015, **23**, (9), pp. 12251–12257
- 32 Cano, E., Allen, B.: 'Multiple-antenna phase-gradient detection for oam radio communications', *Electronics Letters*, 2015, **51**, (9), pp. 724–725
- 33 Zhang, Z., Zheng, S., Chen, Y., Jin, X., Chi, H., Zhang, X.: 'The capacity gain of orbital angular momentum based multiple-input-multiple-output system', *Scientific Reports*, 2016, **6**, pp. 25418